Design and Optimization of Contralateral-type Half-rotating Wing Based on Local Constraint

Li Congmin[1], Wang Xiaoyi[1,a], Li Qian[1], Wang Huixing[1], Qiu Zhizhen[1] and Shan Jianhua[1]

[1]*School of Mechanical Engineering, Anhui University of Technology, Ma´anshan, 243002, P.R.China*

Abstract. Half-rotating wing (HRW) is a kind of similar-flapping wing system based on half-rotating mechanism which could perform rotating-type flapping instead of oscillating-type flapping. Contralateral-type half-rotating wing (CHRW) could run more steadily and smoothly than previous HRW by newly layout of local constraint that mainly consists of moving sheet, circular stator and straight stator. The work principle of CHRW were firstly given in this paper. The design method of key parts local constraint in CHRW was proposed. The contact force model and smooth running condition of moving sheet were especially derived from contact model between moving sheet and circular stator and geometric relation model between moving sheet and straight stator. On the other hand, compared result between theoretical calculation and simulation verified the correctness of contact force model. After optimizing the parameters of some parts of local constraint, the value of contact force was greatly reduced to improve operation stability of CHRW. The research results mentioned above could provide theoretical guidance for design structure of CHRW.

1 Introduction

Flapping-wing air vehicle has been a topic of considerable interest due to its excellent maneuverability and hovering ability [1]. Gradually, many universities and institutes had many research achievements. For instance, the "Micro Bat" [2,3] was developed by California Institute of Technology, and the "DELFLY" [4], a micro flapping wing aircraft, was manufactured by Delft University of the Netherlands. Besides, the "MFI" flapping wing aircraft [5] was from University of California at Berkeley, and a controllable flight flapping-wing machine has successfully developed by Nanjing University of Aeronautics and Astronautics [6]. Driving mechanism is the core component of air vehicle, while excellent driving mechanism is benefit for the stability of aircraft and the reduction of energy consumption. At present, it is difficult for the flapping-wing driving mechanism to get the component simplicity and driving symmetry, which affect the stability of movement and the development of large scale.

Half-rotating mechanism (HRM) [7], an asymmetric rotating mechanism evolved from the basic crank rocker mechanism, provides a new idea for the development of flapping wing driving mechanism. Previously, the traditional HRM was widely used in ship propeller [8] and bionic walking mechanism [9]. With the reasonable improvement and innovation of the HRM, the work team from Anhui University of Technology designed a new kind of HRM that was suitable for flight. It is

[a] Corresponding author: wangxy@ahut.edu.cn

prominent for the development of large scale due to its excellent symmetry and well simplification. Therefore, a more simplified layout and a new local constraint was proposed in this paper on the basis of the original HRW [10]. The CHRW could meet the design requirement by actual operation. Furthermore, the parameters of component which function on the range of local constraint was optimized to improve the life of moving sheet and the stability of CHRW.

2 The layout of CHRW and work principle of local constraint

2.1 The work principle of local constraint

The sketch of HRM was shown in Figure 1, where *H* was a stagnation point. The center point of half-rotation rod (point *C*) whose orientation was always held in the direction of the connection between point *C* and point *H* was connected to the crank endpoint. Half-rotating rod would turn half round when the crank turned one round. The constralateral-type half-rotating mechanism (CHRM) was shown in Figure 2, which was composed of moving sheet, straight stator and circular stator. Both one side of crank (point *C*) and the center of positioning sliding shaft (point *H*) were fixed in frame. In addition, the crank and blade was hinged at point *C* and the blade would slide in groove of positioning sliding shaft when crank was rotated around point *O*. However, the gap between wing blade and groove of positioning shaft brought in the angular deviation which would resulted in irregular movement of blade. Essentially, the contact between moving sheet and circular stator could correct the trajectory of blade by eliminating angular deviation. Meanwhile, the straight stator would play a key role to avoid indeterminate movement of blade when point *C* overlapped with point *H*.

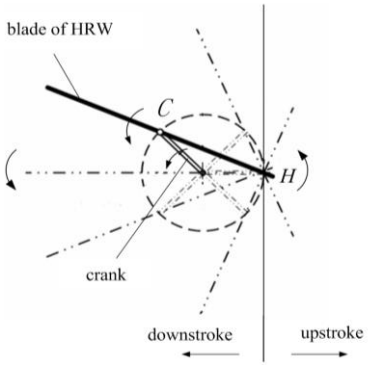

Figure 1. Work principle of HRM

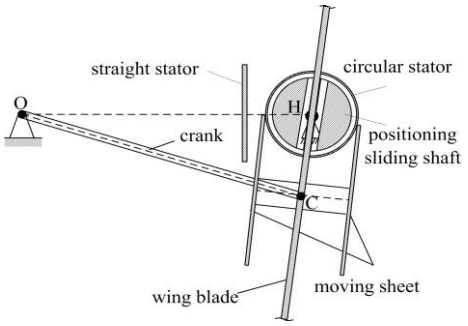

Figure 2. The CHRM with local constraint

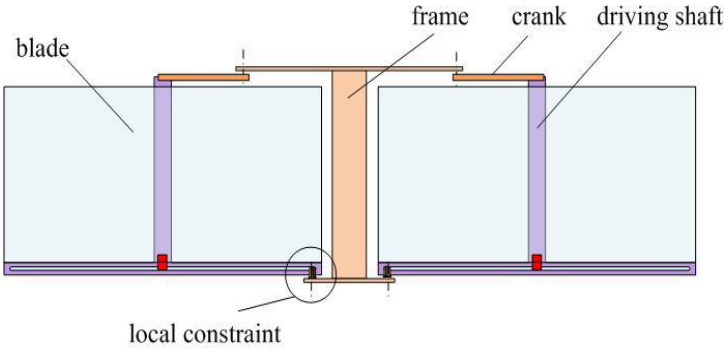

Figure 3. The layout of CHRW

2.2 The layout and movement of CHRW

The layout of CHRW was shown in Figure 3. The crank, blade and local constraint were distributed in both sides of frame, which improved the stress state of the whole frame and mitigated the vibration of CHRW.

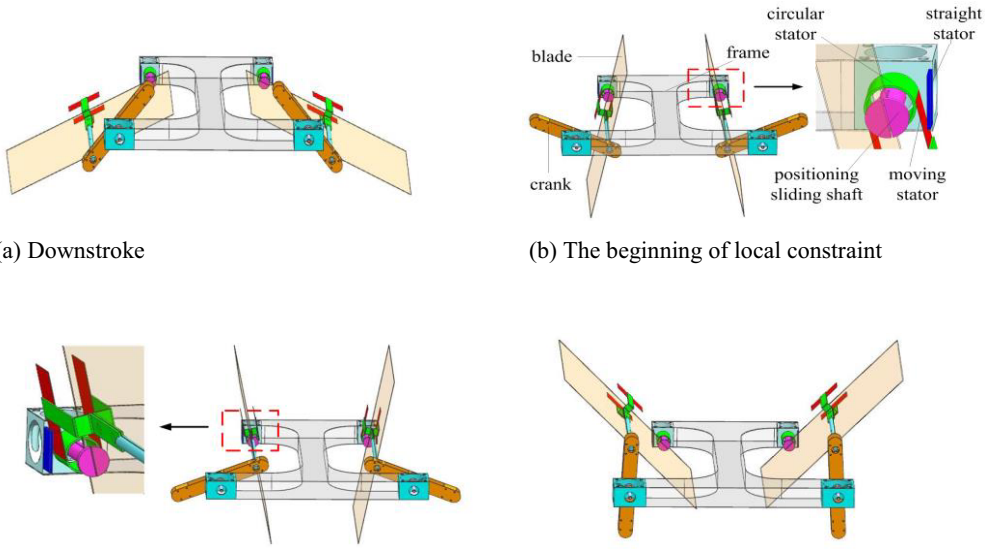

(a) Downstroke (b) The beginning of local constraint

(c) The end of local constraint (d) Upstroke

Figure 4. The movement of simplified constralateral-type HRW in different time

The movement process was shown in Figure 4, which was based on the state of movement and the principle of HRW.

3 Design of local constraint of CHRW

The local constraint was made up of moving sheet, straight stator and circular stator. In this paper, the design of moving sheet was the research emphasis.

3.1 The performing range of local constraint

The gap between blade and groove could be insured with the smooth sliding of blade, but simultaneously it brought in angular deviation which would damage the accuracy of movement for blade.

The angular deviation model was shown in Figure 5. R was the length of crank, φ was the rotating angle of crank, δ was the width of groove and θ represented the angular deviation. The angular deviation could be calculated as follows

$$\theta = \frac{\delta - t}{4R\sin\left|\frac{\varphi}{2}\right|} \tag{1}$$

The angular deviation θ would be increased with the rise of φ. Therefore, a maximum angular deviation θ_m could be set to limit the range of local constraint φ' as

$$-2\arcsin(\frac{\delta - t}{4R\theta_m}) \le \varphi' \le 2\arcsin(\frac{\delta - t}{4R\theta_m}) \tag{2}$$

3.2 Design of circular stator

The angular deviation increased quickly when point *C* closed to the point *H*. Consequently, it is necessary to correct the trajectory of blade and calculate the envelope line of moving sheet primarily.

The coordinate system was established as shown in Figure 6, whose origin was set in point *H*. Moving sheet was located in the line *AB* whose linear equation could be calculated as

$$-x\cos\frac{\varphi}{2}+y\sin\frac{\varphi}{2}=p \tag{3}$$

Where *p* was the perpendicular distance between point *H* and line *AB*.

The equation of envelope line could be got as

$$x^2+y^2=p^2 \tag{4}$$

Obviously, the envelope line of moving sheet was a circle whose center and radius were respectively point *H* and *p*. Consequently, a circular stator was designed according to the above calculation.

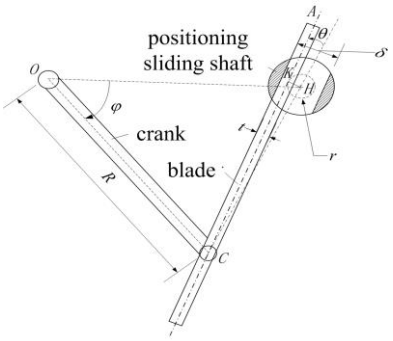

Figure 5. Geometric model of angular deviation

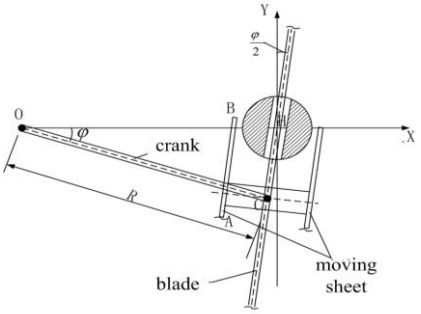

Figure 6. Geometric position of moving sheet

3.3 Design of moving sheet

3.3.1 The velocity of contact for moving sheet

The geometric position of blade in groove was shown in Figure 7. The solid line was the actual position of moving sheet while the dashed line was the theoretical position of moving sheet. The velocity of moving sheet on actual position and theoretical position could be compared to simplify calculation because the calculation of actual velocity for moving sheet endpoint was too complex.

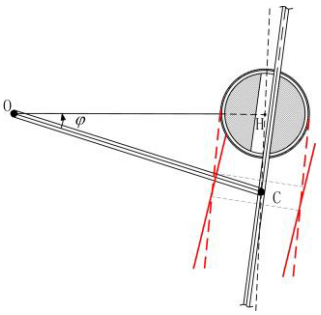

Figure 7. Two kinds of positions for moving sheet

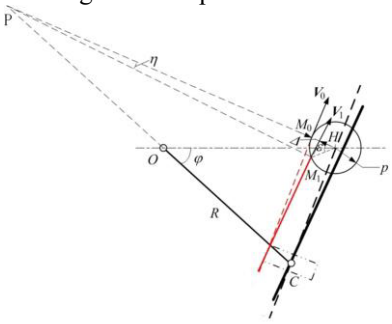

Figure 8. Velocity of moving sheet endpoint

The sketch of velocity was shown in Figure 8. Then point P was the velocity instantaneous center of blade. M_0 was the theoretical position of moving sheet endpoint whose velocity was $\boldsymbol{V}_0$. M_1 was the actual position of moving sheet endpoint whose velocity was $\boldsymbol{V}_1$. In addition, Δ was the deflection of blade. PM_0 was vertical with $\boldsymbol{V}_0$ while PM_1 was vertical with $\boldsymbol{V}_1$. η was the included angle of PM_0 and PM_1. Thereby $\boldsymbol{V}_0$ and $\boldsymbol{V}_1$ were calculated by velocity instantaneous method as

$$\begin{cases} V_0 = PM_0 \cdot \dfrac{\omega}{2} = \dfrac{\omega}{2}\left(2R\cos\dfrac{\varphi}{2} - p\right) \\ V_1 = PM_1 \cdot \dfrac{\omega}{2} = \dfrac{\omega}{2}\left(2R\cos\dfrac{\varphi}{2} - p + \Delta\right) \end{cases} \tag{5}$$

$\boldsymbol{V}_0$ and $\boldsymbol{V}_1$ were compared according to formula (5) and actual parameters of other components to get the result as follows

$$\begin{cases} \dfrac{V_1 - V_0}{V_0} = \dfrac{\Delta}{2R\cos\dfrac{\varphi}{2} - p} \approx 0 \\ \tan\eta = \dfrac{\sqrt{2p\Delta - \Delta^2}}{2R\cos\dfrac{\varphi}{2} - p} < \dfrac{\sqrt{2p\Delta}}{2R\cos\dfrac{\varphi}{2} - p} = \dfrac{\sqrt{\dfrac{2\Delta}{p}}}{\dfrac{2R}{p}\cos\dfrac{\varphi}{2} - 1} \approx 0 \end{cases} \tag{6}$$

The magnitude and orientation of $\boldsymbol{V}_0$ and $\boldsymbol{V}_1$ were extremely close from the above equation, thus $\boldsymbol{V}_0$ could be used as a substitute for $\boldsymbol{V}_1$ in the following calculations.

3.3.2 The contact force between moving sheet and circular stator

The moving sheet would be bended when contacted circular stator since the moving stator was made from elastic metal. The contact model was established to calculate the contact force as shown in Figure 9, where the moving sheet could be regarded as many particles connected by springs.

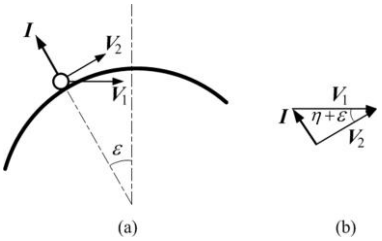

Figure 9. The model of contact

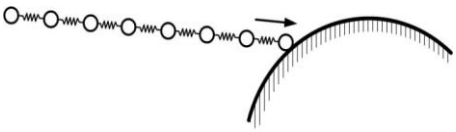

Figure 10. The velocity of contact

The contact velocity was shown in Figure 10. $\boldsymbol{V}_1$ was the velocity before contact whose direction was as same as moving sheet. And then, $\boldsymbol{V}_2$ was the velocity after contact whose direction was tangent to the surface of circular stator. However, it would result in more than one contact if the bending angle of $\boldsymbol{V}_1$ could not reach to $\eta+\varepsilon$. Therefore, $\boldsymbol{V}_2$ was the minimum velocity by the analysis on the above. Momentum theorem could be used to calculate $\boldsymbol{V}_2$ as

$$\begin{cases} I = mV_2 - mV_1 \\ I = \rho A V_0^{\,2} \sin\varepsilon \mathrm{d}t \end{cases} \tag{7}$$

Where $\boldsymbol{I}$ was impulse, m was the mass that participated in the contact part of moving sheet.

In addition, $\boldsymbol{I}$ could also be calculated by equation $I = Fdt$. F was instantaneous contact force of the moving sheet and circular stator. Therefore, F could be calculated as follows

$$F = \rho A V_0^2 \sin(\varepsilon + \theta) = \frac{1}{4}\rho A\omega^2 \left(2R\cos\frac{\varphi}{2} - p\right)^2 \sin\varepsilon \tag{8}$$

Where ρ was the density of moving sheet, A was the cross sectional area, ω was the angular velocity of crank.

3.3.3 Calculation of thickness of moving sheet

It was concluded in section 2.3.2 that $\boldsymbol{V}_2$ was the reasonable velocity for moving sheet when contacted circular stator. The geometric model of contact force was shown in Figure 11.

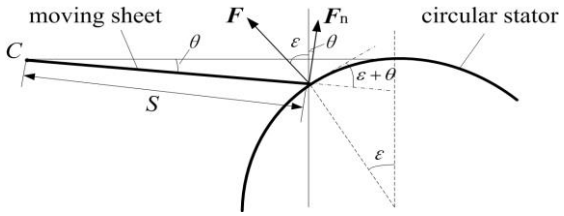

Figure 11. The geometric model of contact force

$\boldsymbol{F}_n$ was the force who bent the moving sheet, it could be calculated as follows

$$F_n = \frac{1}{4}\rho A\omega^2 \left(2R\cos\frac{\varphi}{2} - p\right)^2 \sin\varepsilon\cos(\varepsilon + \theta) \tag{9}$$

The condition of smooth movement for moving sheet was $\frac{F_n S^2}{2EI} = \varepsilon + \theta$, so it was got as

$$\frac{\rho A\omega^2 S^2 \left(2R\cos\frac{\varphi}{2} - p\right)^2 \sin\varepsilon\cos(\varepsilon + \theta)}{8EI} = \varepsilon + \theta \tag{10}$$

Where $I = \frac{1}{12}bh^3$, b was the width of moving sheet, and h was the thickness of moving sheet, so it could be got in this form

$$h = \sqrt{3}\omega S(2R\cos\frac{\varphi}{2} - p)\sqrt{\frac{\rho\sin\varepsilon\cos(\varepsilon + \theta)}{2E(\varepsilon + \theta)}} \tag{11}$$

3.4 Designing of the straight stator

The constraint for blade was disappeared when point C was overlapped with point H, which was not allowed in the design. The straight stator was used to avoid the free movement of blade by missing constraint.

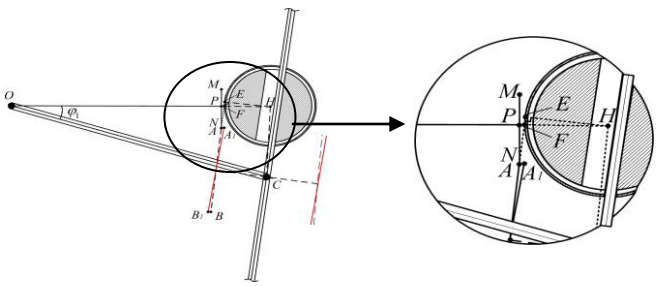

Figure 12. The geometric relation of moving sheet and straight

The geometric relation of moving sheet and straight stator was shown in Figure 12. AB was the theoretical position of moving sheet and A_1B_1 was the actual position of moving sheet. Both positions were almost the same in terms of the calculation by the parameters in above design. Therefore, the actual position could be placed by the theoretical position as

$$l = 2\cos\frac{\varphi_1}{2}(2R\sin\frac{\varphi_1}{2} - S - p\tan\frac{\varphi_1}{2}) \quad (12)$$

Where l was the length of straight stator, φ_1 was the angle of crank when moving sheet and straight stator contacted.

The distance between straight stator and circular stator could be calculated as

$$d = \frac{p}{\cos\frac{\varphi_1}{2}} + \sin\frac{\varphi_1}{2}(2R\sin\frac{\varphi_1}{2} - S - p\tan\frac{\varphi_1}{2}) - p \quad (13)$$

The parameters of straight stator could be calculated from parameters of moving sheet and circular stator. Besides, φ_1 could be provided in accordance with technical condition.

4 Simulation and optimization of contact force between moving sheet and circular stator

4.1 Simulation of contact force

The contact force could be calculated by formula (8). Four sets of parameters were proposed in Table 1, which was calculated by four groups parameters based on theoretical analysis and calculation in section 2. Meanwhile, ADAMS was used in simulating the contact force in order to verify the theoretical result.

Table 1. Comparison of theoretical contact force and simulation contact force under different local constraints

Group	b (mm)	t_1 (mm)	l_1 (mm)	r (mm)	δ (mm)	t_2 (mm)	Contact force value by calculation (N)	Contact force value by simulation (N)
a	26.5	0.18	25	10	0.6	0.4	0.27	0.30
b	30	0.21	28	12	0.7	0.4	0.34	0.40
c	40	0.3	26	13	0.6	0.2	0.63	0.60
d	30	0.22	25	10	0.65	0.4	0.42	0.45

In the Table 1, b, t_1 and l_1 were respectively the width, thickness and length of moving sheet. Besides, r was the radius of circular stator, δ was the width of groove and t_2 was the thickness of blade.

After comparing theoretical calculation and simulation results, the conclusion could be got that the contact force model was reasonable.

4.2 Optimization of contact force

High-speed movement of blade in operation caused the high-frequency contact between moving sheet and circular stator. It was necessary to optimize the contact force to extend the life of moving sheet and improve the stability of half-rotating blade.

4.2.1 Design variables

The design variables must be independent as

$$\boldsymbol{X} = (X_1, X_2, X_3, X_4, X_5, X_6) = (b, t_1, l_1, r, \delta, t_2) \quad (14)$$

4.2.2 Objective function

High-frequency contact was harmful to moving sheet and circular stator so that the minimum contact force was chosen as objective function as

$$\min f(X) = F \tag{15}$$

4.2.3 Constraint condition

$$g_1(x) = \sqrt{\frac{X_5 - X_6}{X_4}} + \frac{X_5 - X_6}{2X_3} - \frac{6.4\times10^{-10}}{X_2^{\,2}}[X_3^{\,2}(120\sqrt{1-\frac{X_3^{\,2}}{14400}} - X_4)^2\sqrt{\frac{X_5 - X_6}{X_4} - \frac{(X_5 - X_6)^2}{4X_4^{\,2}}}] \le 0$$

$$g_2(x) = \sqrt{X_4^{\,2} + X_3^{\,2}} - 60 \le 0$$

$$g_2(x) = \sqrt{X_4^{\,2} + X_3^{\,2}} - 60 \le 0$$

$$g_4(x) = \frac{X_4}{\sqrt{1-\frac{X_3^{\,2}}{14400}}} - X_3 \le 0 \tag{16}$$

$$g_5(x) = X_4 - X_3 \le 0$$

4.2.4 Comparison of the contact force before and after optimization

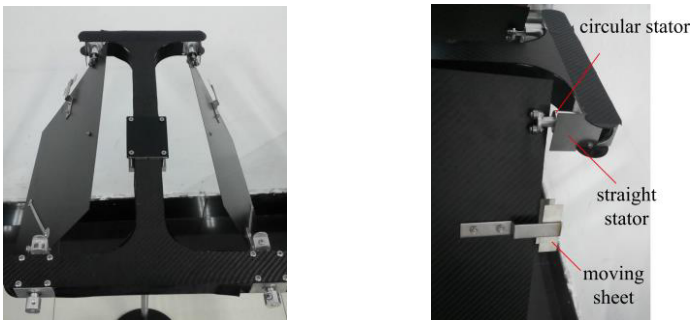

Figure 13. The prototype of CHRW

The prototype of CHRW was shown in Figure 13. Then the function of "fmincon" from MATLAB was used to optimize the parameters of the driving mechanism and the parameters before and after optimization were shown in Table 2. It could be indicated that the contact force reduced about 33.9% after optimization.

Table 2. The result before and after optimization

	b (*mm*)	t_1 (*mm*)	l_1 (*mm*)	r (*mm*)	δ (*mm*)	t_2 (*mm*)	force (*N*)
before	26.5	0.2	26	10	0.8	0.5	0.321
after	28	0.145	30	9.3	0.63	0.42	0.212

5 Conclusion

(1) The contralateral-type layout and local constraint was designed based on the principle of HRM, which included calculation of size and position for moving sheet, circular stator and straight stator.

(2) The contact model of the moving sheet and circular stator was established based on the momentum theorem, which was verified by four contact models in ADAMS.
(3) The dimension parameters of working part who toke part in the local constraint was optimized in MATLAB. The contact force reduced about 33.9%, which obviously extended the lives of moving sheet and circular stator, at the same time improved the stability of CHRW.

Acknowledgments

This work is supported by the National Natural Science Foundation of China (Grant No. 51375014 and No. 51405001)

References

1. Wood RJ. The First Take off a Biologically Inspired At-scale Robotic Insect [J]. IEEE Transactions on Robotics, 24(2): 341-347(2008)
2. Mueller J. Fixed and Flapping Wing Aerodynamics for Micro Air Applications [M]. Virginia: American Institute of Aeronautics and Astronautics(2001)
3. Pornsin-Sirirak TN, Lee SW. MEMS Wing Technology for a Battery-powered Arnithopter [C]. The 13th IEEE Annual International Conference on MEMS, 799-804(2000)
4. De Croon G C H E, De Wagter C. Design, Aerodynamics and Vision-Based Control of the DflFly [J]. Internatioanl Journal on Micro Air Vehicles. 1(2) : 71-97(2009)
5. Schenato L, Deng X, Wu W C, et al. Virtual Insect Flight Simulator (VIFS): A software tested for insect flight [C]. Seoul(2001)
6. Zhu B. Research on flapping-wing flight mechanism and bionic flapping-wing mechanism [D]. Nanjing: Nanjing University of Aaeronautics and Astronautics(2010) (in Chinese)
7. Qiu Z Z, Half-Rotating Mechanism: Structure, Characteristics and Application, Hefei: University of Science and Technology of China(2011) (in Chinese)
8. Y H Zhang，Z Z Qiu. Propeller with a Blade and its Motion Characteristics [J]. Chinese Journal of Mechannical Engineering, 42 (3): 193~196(2006) (in Chinese)
9. X Y Wang, L L Mei. Analysis and Application of Motion Geometry Feature for a New Biped-imitating Walking Mechanism [J]. Mechanical Science and Technology for Aerospace Engineering, 30 (6): 1020~1024(2011) (in Chinese)
10. Wang X Y, Zhang Y Q, Wang H X, et al. Research of Local Constraint for Simplified Half-Rotating Mechanism[J]. Applied Mechanics & Materials, 826:35-39(2016) (in Chinese)